TRADE CUMULUS: OBSERVATIONS AND MODELLING

ALAN K BETTS
Atmospheric Research
RR3, Box 3125, Pittsford, VT 05763
akbetts@aol com

1. Introduction

This talk reviews some work on convective boundary layer (CBL) equilibrium and radiative-convective equilibrium in the Tropics It is based primarily on *Betts and Albrecht* [1], *Betts and Ridgway* [2] [3] and on the use of conserved thermodynamic variables, as discussed in several papers (eg *Betts* [4] [5] [6] [7] [8] [9] [10]).

A convective boundary layer (CBL) of shallow non-precipitating cumulus clouds covers most of the tropical oceans away from the atmospheric convergence zones. It is remarkably uniform with the cloud-base near 950 mb, an inversion above the top of the cloud layer near 800 mb (eg *Firestone and Albrecht* [11]); and a subcloud layer equivalent potential temperature θ_e, typically in the range 345-350K. This boundary layer in turn feeds the deep convection in the ascending branches of the Hadley and Walker circulations, so that *the height of the tropopause and tropical tropospheric temperature are directly coupled to the* θ_e *of the CBL over the oceans* (*Sarachik* [12]). This rather stable equilibrium is a result of a subtle balance between the radiation field, the subsidence, the convective fluxes, the cloud field, the surface wind and the sea surface temperature. Many timescales are involved. For this talk I shall address this equilibrium balance on two timescales over the oceans, using a simple energy balance model. We shall explore the dependence of the equilibrium low level θ_e, height of cloud-base and CBL top, and the surface fluxes of heat and moisture, on sea surface temperature, surface wind speed, and the moisture above the CBL. The early studies of the Tradewinds emphasized the downstream moistening and rise of the top of the cloud layer on equatorward trajectories towards Hawaii (*Riehl et al.* [13], *Malkus* [14]) We shall show this is largely an equilibrium response to the rise of sea surface temperature along the trajectory. Over most of the tropical Pacific where the sea surface temperature has weaker gradients, the CBL top is near 800 mb. These early papers used kinematic methods to estimate the mean subsidence in the Trades and found values ≈ 6 mb day^{-1}, much lower than that required for mass balance in the subsiding branch of the Hadley circulation. *Neiburger* [15], however, used trajectories and a radiative budget to estimate the subsidence at CBL top to be ≈ 40 mb day^{-1} Subsequent mass budget studies of the Tradewinds in the Atlantic (*Holland and Rasmusson* [16], *Nitta and Esbensen* [17], *Augstein et al* [18]) confirmed that the subsidence in the Trade inversion was of order 40-60 mb day^{-1} Papers [12] and [2] showed that the radiatively driven subsidence in the subsiding branches of the mean tropical circulation was of this same magnitude ≈ 40 mb day^{-1} Paper [2] used a

R. K. Smith (ed.), The Physics and Parameterization of Moist Atmospheric Convection, 99 126.

coupled radiative-CBL model and observed CBL data over the equatorial Pacific (from [1]) to show that on climatic timescales, the radiation field was the primary control on the surface fluxes.

1.1 THE ISSUE OF TIMESCALE AND THE PARAMETERIZATION PROBLEM

From a modelling and observational perspective, the key issue for the CBL is, I believe, whether we can predict the correct equilibrium thermodynamic state (which I shall represent by potential temperature θ, and mixing ratio q) in situations over land and sea that are changing slowly; and the correct rates of change for CBL's forced from the surface; such as the diurnal cycle over land, or the advection of cold air over a warmer ocean. In this verbal definition, we immediately see the essential issue of timescale, so I shall first discuss the internal and external timescales (τ_I , τ_E) for the CBL. This separation is for conceptual convenience. The external or boundary timescales are those which determine the fluxes at the surface (surface wind and temperature, roughness; soil moisture, vegetation over land etc) and at CBL top (entrainment of air from above). The radiative process also has a comparable timescale to entrainment (*Betts* [19]). The internal timescale is the timescale of mixing within the CBL. There may be different values for the cloud and subcloud layers. If $\tau_I << \tau_E$, then the CBL will have a nearly well-mixed structure, and correspondingly mixed layer models are useful simplifications. However even if a CBL is nearly well-mixed, its equilibrium state or time-change will not be correctly predicted in a model, if the boundary fluxes are wrong. Superficially the surface flux problem over the oceans is easier than over land (but still a problem at low wind speeds (eg. *Miller et al.* [20])). Over land, the surface fluxes during the daytime depend on the vegetation and soil moisture (and their time history) and the net radiation (which is controlled on a short time-scale by CBL cloud). The entrainment fluxes are not well-known, either for cloud-free BL's [9], or for cloudy CBL's. This is because entrainment is not really external at all. It is driven by the circulations within the BL or within clouds, and may well differ significantly for circulations driven by surface fluxes, or radiative processes interacting with the cloud layer.

But if we continue the conceptual separation of internal and external timescales a little longer, we can say that the ratio τ_I / τ_E controls how well-mixed a CBL is. This is important because it has a connection to cloud fraction. Well-mixed BL's over the ocean will generally always be capped with stratocumulus [10]; while trade cumulus layers which have $\tau_I \approx \tau_E$ (and therefore are poorly mixed) have small cloud fractions. But since the clouds are the agent of mixing in CBL's, and their presence interacts with the radiation field to drive more mixing internally (as well as reducing surface net radiation over land); the coupling and feedback between the boundary fluxes, the internal structure and the cloud field is so tight, that it is not surprising that our attempts at parametrization have had so far only limited success in GCM's.

The next section is a review distilled from some of my earlier papers on the use of conserved variable mixing diagrams in the study of the tradewind CBL.

2. Tradewind Boundary Layer Equilibrium

2.1. TRADEWIND CUMULUS ON MIXING DIAGRAMS

The conserved variable diagram I shall use is a plot of saturation potential temperature against saturation mixing ratio [5] [8] [9]. Figure 1 shows this diagram with superimposed lines of saturation pressure (solid) from 1000-600 mb. Shown are three important reference processes: the wet adiabat (solid) of θ_{es} = 350 K, the wet virtual adiabat (dotted) of 350 K (which is the neutral stability line for cloud parcels rising adiabatically, including the density effects of liquid and water vapor), and the dry virtual adiabat of θ_v = 300 K (which is the neutral stability line, including the density effect of water vapour in unsaturated parcels). The x axis is of course the dry adiabat of constant θ on this Figure, and the y axis is a line of constant q.

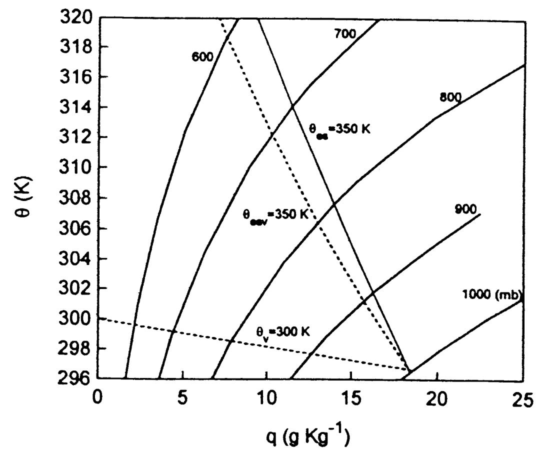

Figure 1. Conserved variable diagram (θ^*, q^*), showing constant saturation pressure lines, wet adiabat (solid), wet and dry virtual adiabats (dotted).

Figure 2 shows an example of the mean structure of a tradewind CBL in the Equatorial Pacific from [1]. (Consider Figure 2 superimposed on Figure 1.) The markers are saturation points (SP) for this mean sounding at 10 mb levels, from saturation at the ocean surface pressure of 1010 mb on the far right to a pressure of 600 mb (with a saturation pressure p^* of 505 mb) on the far upper left. This is a characteristic thermodynamic distribution through an oceanic tradewind CBL. There is a weakly superadiabatic layer above the surface where θ falls ≈ 1.2 K, and q falls ≈ 5.5 gKg^{-1}: this appears as a jump in this data between the ocean surface data point at 1010 mb and the first atmospheric point at 1000 mb, which has a saturation level near 960 mb, corresponding to the tradewind cloud-base. There is a clustering of points near this saturation pressure, corresponding to air in the subcloud layer with 1000 > p > 970 mb. This subcloud layer air is nearly well mixed; the timescale of mixing is quite fast (≈1000 sec), because small perturbations in θ_v generate vertical velocities ≈ 1 ms^{-1} and its depth is only 500 m. Correspondingly, note that the

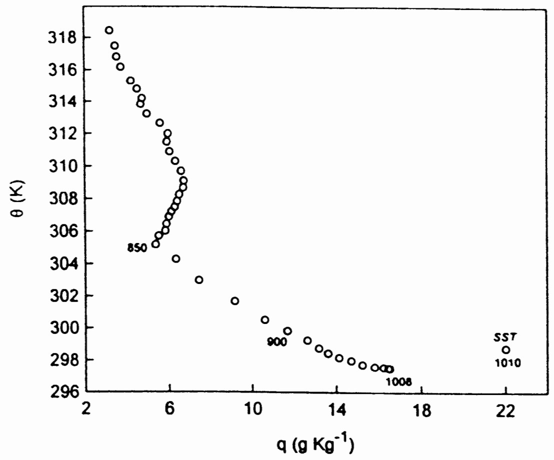

Figure 2. (θ, q) plot for E. Equatorial Pacific average (#141) from [1].

distribution of SP from 1000 to 960 mb is parallel to a θ_v isopleth, the neutral density line. Above cloud-base, there is a smooth gradient of SP in the lower part of the trade-wind cumulus layer, which is less well mixed than the subcloud layer, and then a more rapid transition from say 900 to 850 mb which corresponds to the trade inversion. This partially mixed cumulus layer has a structure on this (θ, q) plot that is nearly linear, corresponding to a mixing line, with a slope between the dry and wet virtual adiabats. This is characteristic of partly cloudy CBL's. At 850 mb, the top of the inversion, the sounding has a sharp kink, where moisture increases with height at nearly constant $p^* \approx 670$ mb. This air has probably subsided (with radiative cooling) on timescales of order 5-6 days, after exiting a deep convective system near the freezing level in the mid-troposphere [1].

Now consider this CBL as an equilibrium between the surface fluxes, the entrainment fluxes and net radiative cooling. The subcloud layer equilibrium is a balance of four vectors (see [7] [10]) shown schematically in Figure 3: a surface flux (driven by the surface wind) which moves this layer towards saturation at the ocean surface, a flux through cloud-base (the upward transport of moisture and downward transport of heat through cloud-base), radiative cooling, and a small vector for the effect of subsidence on this layer. At equilibrium, over 90% of the surface moisture flux is transported through cloud-base, and the surface and cloud-base heat fluxes together closely balance the radiative cooling (which is large for the moist subcloud layer over the tropical oceans ($\approx$-2.4 K day^{-1})). We can see that the subcloud layer is kept cooler than the ocean by this radiative cooling. The formal construction of this diagram can be summarized briefly as follows. The surface flux vector can be represented as a vector difference of SP's (saturation points) in terms of a bulk aerodynamic formula $g F_o = \omega_o \Delta S$
where

$$\Delta S = \Delta(C_p \theta, Lq) \qquad (1)$$

and $\omega_O/g = \rho_O C_T V_O$ (density, bulk transfer coefficient and wind-speed). The same velocity scale (ω_O/g) is then used to represent the other fluxes: for example, the length of the radiative cooling vector $(\Delta\theta_N)$ is

$$C_p(\omega_O/g)\Delta\theta_N = \Delta R_N \qquad (2)$$

where ΔR_N is the net radiative flux difference across the subcloud layer. Typically $\Delta R_N \sim 15 Wm^{-2}$, $\omega_o \sim 80\, mb/day$ giving $\Delta\theta_N \sim 1.6\, K$. In Figure 3 the cloud-base vector and subsidence vectors are schematically drawn from the budget estimates made in section 3.

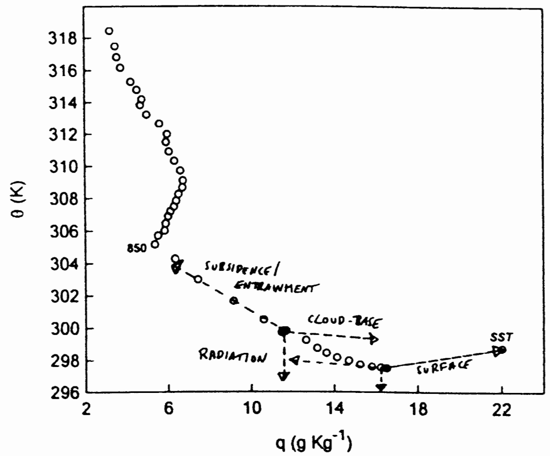

Figure 3. As Fig 2 with schematic vector diagrams for thermodynamic balance of cloud and subcloud layers.

The tradewind cloud layer is not well-mixed. The air transported through cloud-base with the properties of air from say 1000 mb is distributed through the cloud-layer with a cloud mass flux that decreases with height [4] [8]. *Betts* [6] showed how the decrease and rotation of the cloud thermodynamic flux vector with height can balance the net radiative cooling, layer by layer, and produce the smooth change in structure that we also see here. The cloud layer is not well mixed, but if we integrate over it (from 850-960 mb), we can schematically show the equilibrium of the whole layer as the vector balance shown. The heavy dot at $(\theta, q) = (300.1\, 8K, 11.4 gKg^{-1})$ is the mean SP of the cloud layer. Its equilibrium is a balance of the cloud-base flux (direction reversed), the subsidence of warm, dry air into the layer (this is mixed downwards by the clouds, so that the trade inversion is maintained with a top at 850 mb, as the air at this level subsides in balance with the radiative cooling), and the radiative cooling ($\approx$30 Wm^{-2}) of the cloud layer itself.

The subcloud layer is nearly well mixed because its internal mixing timescale τ_{Bl}) is much shorter than the surface flux timescale of $\tau_b \sim \Delta p_s/\omega_O \sim 50/80 \sim 0.63\, days$.
We can estimate τ_{Bl} roughly from the surface convective velocity-scale

$$\omega_{O^*} = g\left(\frac{\bar{\rho}F_{O\theta}\Delta p_B}{C_p\theta}\right)^{1/3} \approx 5.5\,Pa\,s^{-1} \approx \;5000\; mb\; day^{-1}$$

where F_{θ} is the surface heat flux ($\approx 10\,W m^{-2}$), and Δp_B is the pressure thickness of the subcloud layer of 50 mb. In the dry convective layer, regions of ascent and descent are roughly equal, so we can estimate the internal circulation time-scale as the subcloud layer $\tau_{Bl} = 5000/\omega_{O^*} = 1000$s (or 15 mins). Since $\tau_{Bl} << \tau_o$, the subcloud layer is nearly well mixed.

However for the cloud layer, the internal timescale is much longer. An estimate can be made from the convective mass flux. Near cloud-base this may be as high as 300 mb/day, falling to below 50 mb/day near the inversion-base (see section 3). Correspondingly the internal timescale for mixing in a 100 mb thick cloud layer would rise with height from ≈ 0.33 days in the lower cloud layer to over one day in the inversion layer (see section 3). Qualitatively the wider spread of SP in Figure 2 in the inversion layer reflects this.

2.2. MASS FLUX MODEL FIT TO TRADE CUMULUS EQUILIBRIUM

Figure 2 shows the equilibrium structure of a tradewind layer in the eastern equatorial Pacific. *Betts and Ridgway* [2] showed how the surface fluxes could be retrieved using a radiation model to estimate the radiatively driven subsidence at CBL-top, and then a mixing line model to represent the internal structure of the CBL. I will reproduce a simplified version of this analysis here for illustration, and reconstruct the convective fluxes from the surface through the CBL, together with the convective mass flux distribution in the cloud layer. A mean subsidence ($\bar{\omega}$) is first assumed with a magnitude consistent with [2]. This has a simple structure: the subsidence is fixed at 40 mb/day in the cloud layer ($960 < p < 850$) and decreases linearly below cloudbase to zero at the surface (1010 mb). The simplified one dimensional moisture budget equation is then solved to give the convective flux of total moisture, which balances the subsidence (using the observed mean moisture structure

$$F_{q^*}(p) = L\int_{850}^{p} \bar{\omega}(\partial\bar{q}/\partial p)\,dp/g \qquad (3)$$

This gives a surface moisture flux of 128 Wm^{-2}, and a cloud-base flux of 117 Wm^{-2}, both realistic values. The profile is shown in Figure 4.

If we then use the subsidence and the mean $\bar{\theta}(p)$ structure, we can estimate the radiative cooling rate which will satisfy the energy balance of the cloud and subcloud layers. We find (again consistent with [2]) that this needs a mean radiative cooling of $\dot{\theta}_R = -2.4$ K/day to give a realistic surface flux. We use this value independent of height to retrieve a convective θ^* flux from

$$F_{\theta^*}(p) \doteq C_p\int_{850}^{p} (\bar{\omega}\partial\bar{\theta}/\partial p + \dot{\theta}_R)\,dp/g \qquad (4)$$

This gives a surface heat flux of 10 Wm^{-2} and a cloud-base value of -4 Wm, and a reasonable distribution with height through the cloud layer. Figure 4 shows the vertical structure of these convective fluxes. They are very similar to those derived from the BOMEX data by [16][17] and [4]. A bulk aerodynamic formula

$$F_{Oq^*} = L(\omega_o/g)(q_s(SST) - \bar{q}(1000)) \qquad (5)$$

gives a value of ω_O of 80 mb/day corresponding to a surface windspeed of 5.2 ms^{-1} with a surface transfer coefficient of 1.3 10^{-3} (realistic for this region). The same value of ω_O gives an estimate of the $F_{O\theta^*}$ from the SST and air temperature of 11.5 Wm^{-2}, which is sufficiently close to our budget value assumed in (4).

A convective mass flux can also be retrieved from the moisture flux using

$$F_{q^*}(p) = \omega^*(p)(q_c - \bar{q}) \qquad (6)$$

We assumed q_c constant equal to 16.54 gKg^{-1} (the value found near the base of the subcloud layer), and derived the profile of $\omega^*(p)$ also shown in Figure 4. The cloud-base value is near 300 mb day^{-1}, falling rapidly with height, as shown by earlier studies. A similar estimate can be derived from $F_{\theta^*}(p)$, but the cloud-base mass flux is very sensitive to errors of ± 0.1 K in the value of θ_c chosen, since both the θ flux and $(\theta_c - \bar{\theta})$ are small near cloud-base. However, we can say that, given a plausible value of θ_c, the convective mass flux profile derived using (6) (from the moisture flux) will match the θ^* flux from (4) to < 2 Wm^{-2}.
The derivative of (6) with respect to pressure, which is the convective forcing term, is informative.

$$\frac{\partial F}{\partial p} = \omega^*\left(\frac{\partial\bar{q}}{\partial p}\right) + \left(\frac{\partial\omega^*}{\partial p}\right)(q_c^* - \bar{q}) \qquad (7)$$

since we assumed q_c constant. This shows that the convective flux can be resolved into two terms; a compensating subsidence of the environment related to the convective mass flux ω^*, and a detrainment $(\partial\omega^*/\partial p)$ of air with cloud properties q_c^* (total water) to the environment. There is a corresponding θ^* equation.

The compensating subsidence term is a warming and drying, while the detrainment term is a cooling and moistening (since the clouds have greater total water and their liquid water evaporates. Figure 4 shows where the terms are dominant. In the enthalpy budget, the slope

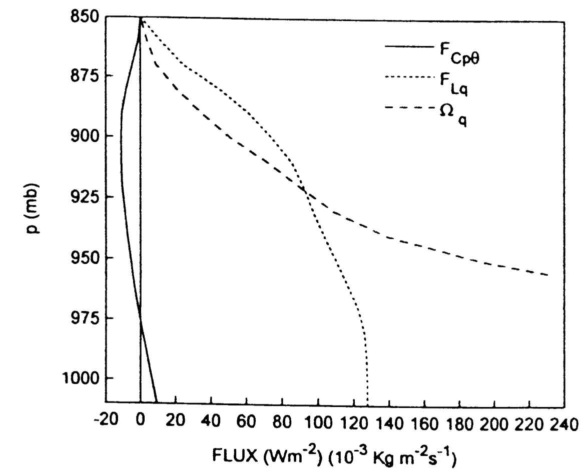

Figure 4. Convective fluxes (solid) derived from profiles in Fig. 2, assuming subsidence and radiative cooling in CBL. Convective mass flux (dashed) derived from moisture flux.

of F_{θ}. changes sign at the inversion base near 890 mb. The inversion layer is cooled because the detrainment of air of low saturated potential temperature θ^* (low because of its liquid water content: originated at cloud base) is the dominant term. In the lower cloud layer the subsidence warming term dominates. The slope of F_q. shows that the cloud field moistens at all levels; at the largest rate in the inversion layer.

3. Convective Boundary Layer Equilibrium over a Tropical Ocean

3.1. INTRODUCTION

In this section, which is abbreviated from [3], a thermodynamic model for a partially mixed CBL (with a specified cloud fraction) is coupled to a radiation model to compute equilibrium solutions for a tropical CBL, and troposphere in energy balance with increasing degrees of coupling. The balance between the radiation field and the CBL structure is quite complex, because radiative cooling has several roles. Above the CBL, the subsidence is close to radiative balance. This subsidence continually brings down dry and warm air into the CBL. For the CBL as a whole, radiative cooling largely balances the warming by subsidence (and the smaller surface sensible heat flux); while the upward advection and evaporation of liquid water maintains the sharp temperature inversion [4], [21]. Over a uniform ocean, it is the radiative cooling that keeps the subcloud layer cooler than the ocean. This maintains the surface layer instability, and the surface sensible (and latent) heat fluxes. In the moisture balance, the subsidence of dry air is balanced by the upward flux of moisture at the surface. The resulting equilibrium moisture structure and associated cloud fields play an important role in controlling the long wave radiative cooling and the net incoming shortwave radiation. Finally the balance of the net incoming radiation and the fluxes of sensible and latent heat at the surface (as well as the oceanic heat transports) determine, on long time scales, the sea surface temperature (see [3]).

After introducing the boundary layer model and the energy balance constraints, this paper first shows the sensitivity of the CBL equilibrium structure and fluxes to external parameters, such as sea surface temperature (SST), surface wind, and a specified upper tropospheric structure and subsidence. The timescale of this response is of order a day (*Schubert et al* [22]). We shall call this the "CBL timescale"; and all the solutions with a specified SST and troposphere above the CBL, the "uncoupled" solutions. We then introduce energy balance for the troposphere, and couple the temperature and moisture structure of the troposphere to the low level θ_e, to give "tropospheric coupled" equilibrium solutions for the CBL. These are representative of a "tropospheric radiative timescale" of order 10 days. On this timescale we shall still regard the SST as an independent specified parameter. This class of solutions show the coupling of CBL structure and fluxes to specified surface wind and SST on the 10-day timescale. The equilibrium of the sea surface temperature (SST), and the ocean mixed layer is a longer timescale (>100days) process, discussed in [3], and *Sui et al.* [23].

3.2. THEORETICAL MODEL

3.2.1. *Concept*

The model is an extension of [2], which was itself based on the single cell model for a tropical circulation in equilibrium proposed by [12]. Figure 5 shows the schematic circulation of this single-cell tropical model with a characteristic set of parameters for illustration (from our coupled equilibrium solution: discussed later). We suppose that most of the tropics are covered by a uniform CBL, above a uniform ocean. This is the region we model; not the narrow ascending branch of the deep convection. Figure 5 shows a characteristic set of fluxes, and the radiative flux divergences for the subcloud layer, ΔN_B, the CBL, ΔN_T, and the troposphere ΔN_{TR}, which will play an important role in the budget analysis. We shall neglect X_A (marked with asterix), the atmospheric export from the tropics, because it is partly balanced by the warming effect of upper level clouds which we also neglect. (In [3] we specified X_O, the oceanic export, to give a realistic SST with a specified cloud fraction consistent with observations, but here we shall specify SST).

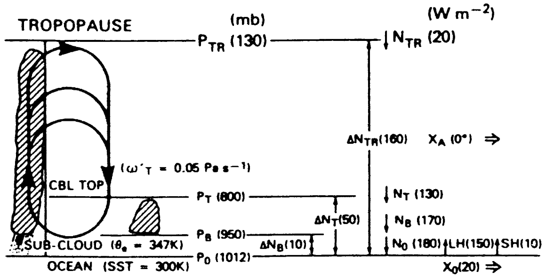

Figure 5. Schematic showing single cell tropical circulation, and selected values from the equilibrium solution with a coupled atmosphere and ocean (see text).

In this section we shall outline the components of the model in turn. The primary focus of the paper is the CBL equilibrium on different timescales. The CBL model is based on the mixing line representation of clear and cloudy thermodynamic profiles for a shallow cumulus layer suggested in [8], [24], and discussed in the next section. The surface fluxes are parameterized by bulk aerodynamic formulae. The troposphere above the CBL has a moist adiabatic ***temperature*** structure, which in the troposphere coupled solutions lies on the moist θ_{es} adiabat through a low level θ_e, (2mb above the surface) and in the uncoupled CBL solution follows a specified moist adiabat. The tropospheric moisture *profile* above the CBL is specified, and in the coupled solutions it is linked to the low level θ_e also. One simplification we shall make is to specify a tropical stratosphere with a constant temperature of 195K between 100mb and the tropopause. The tropopause is at the pressure where the θ_{es} adiabat for the troposphere reaches 195K, and is typically in the range 110-150mb as θ_e decreases. The radiation model is discussed in [2] and [3]. It is used to compute net short-wave and long-wave fluxes for a clear atmosphere, and one with a specified fraction of plane parallel clouds in the CBL.

The CBL heat and moisture budgets and three energy balance criteria are used to give equilibrium solutions. The CBL thermal budget gives an equilibrium solution for the boundary layer depth in terms of the radiative cooling of the CBL, and the subsidence and temperature at the CBL top. We use a subcloud layer energy balance criteria as a constraint on the surface sensible heat flux, and Bowen ratio. Energy balance for the troposphere determines the subsidence at CBL top, and the CBL equilibrium structure on the atmospheric radiative timescale of order 10 days (section 3.2.7).

3.2.2. *Mixing line model for an idealized CBL*

The CBL is typically not well mixed, particularly above cloud-base. To simplify the problem, but give relative profiles, we approximate its bulk thermodynamic structure by a mixing line representation [5] [6] [8]. This has been used as a parameterization for shallow convection in GCM's [24]. Idealized but quite realistic thermodynamic profiles can be constructed with a mixing line model, using different bulk parameters to represent clouds and the clear regions between them. Figure 6a (from [3]) shows example profiles on a thermodynamic diagram for the tropospherically coupled solution with SST = 300K.

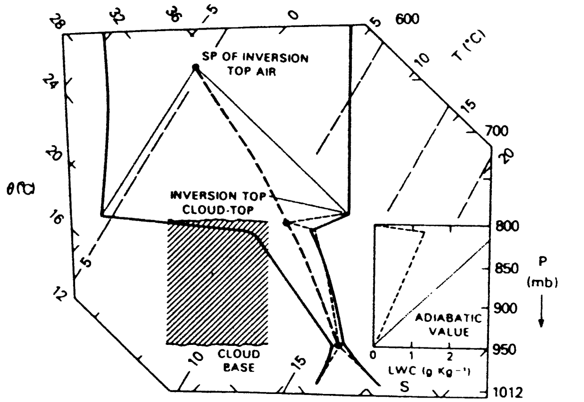

Figure 6a. Tephigram showing CBL model thermodynamic structure. The clear air temperature and mixing ratio are shown as heavy solid lines, and the cloudy air profiles by short dashed lines (the liquid water profile as an insert). The mixing line between the base of the subcloud layer (2mb above the sea surface) and the air above the inversion is shown as a heavy dashed line.

A mixing line (heavy dashes) is computed between air near the ocean surface with properties θ_{MO}, q_{MO}, and the air just above the CBL with properties θ_T, q_T see [5]. All the air in the CBL is presumed to have thermodynamic properties lying on this mixing line. We then construct the thermodynamic profiles for clear and cloudy air within the CBL by specifying different profiles for a parameter

$$\beta = dp^*/dp \tag{8}$$

the change of saturation level with pressure along the mixing line [6] [8]. We compute separate clear and cloudy profiles by using two pairs of values for ß. For the clear air environment between clouds (solid lines in Figure 6a) we specified $\beta_u = 0.2, 1.2$ respectively below cloud-base and above cloud-base (up to the inversion base), consistent with observations of the CBL structure over the oceans [1]. The resolved inversion layer

thickness was fixed at 20 mb, with a linear transition of p^* across it. Figure 6b shows the construction of these environmental profiles of (θ, q) from the mixing line using the same co-ordinates as Figure 2. The four SP's on the (heavy dashed) mixing line corresponding to each pair of (θ, q) points is shown.

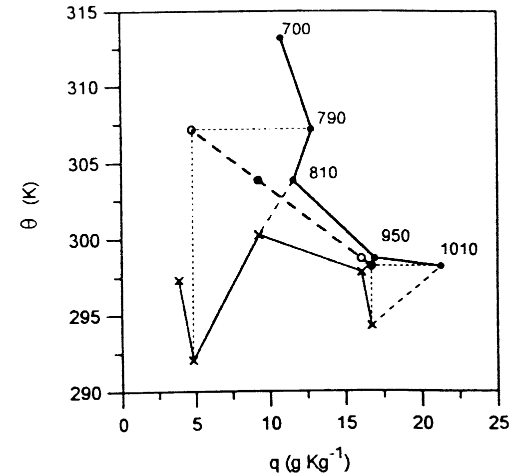

Figure 6b. (θ, q) plot showing relation of parameterized environmental profiles through the CBL to the mixing line.

For the cloudy CBL profiles (short dashes in Figure 6a), we specified $\beta_c = 0.0, 0.6$ respectively below cloud-base and in the cloud layer (up to the inversion base). The value of $\beta_c = 0$ gives a well-mixed subcloud layer beneath clouds, so that cloud-base (generally not a model level) corresponds to the LCL of the air just above the surface. Above cloud-base, $\beta_c = 0.6$ gives a cloud layer liquid water profile that is 40% of the adiabatic value, (corresponding to $1-\beta_c$) to represent the subadiabatic values typical of shallow cumulus clouds. The inset on Figure 6a shows this liquid water profile. Cloud liquid water is specified to fall to zero (where $p^* = p$), 10 mb above the inversion base, so that we have a well defined cloud-top at the middle of the inversion, where the temperature of the evaporating cloud-top can be computed. (It is used in the radiative code). This temperature lies, as shown, on the mixing line at the cloud-top pressure [5].

As Figure 6a shows, this representation gives us idealized but realistic clear and cloudy profiles: with a nearly well mixed subcloud layer, and a conditionally unstable cloud layer capped by an inversion. It can be regarded as an extension of the mixed layer CBL to a partially mixed structure. This is still a bulk parameterization of the CBL, because we *specify* the values of ß, to be consistent with observations of CBL structure. Our results are not very sensitive to this specification. The value of a bulk parameterization is that it gives us realistic thermodynamic profiles (including liquid water) for the radiation computation, which depend only on four *boundary* parameters θ_{MO}, q_{MO} and θ_T, q_T, which can be computed from the budget equations. The mixing line representation gives simple integrated CBL thermodynamic budgets, and it is sufficiently simple to be used to parameterize shallow convection in large-scale numerical models [24]. Our model vertical resolution was fixed at 10mb within the CBL for the computation of the radiative fluxes. The solution of the budget equations (see sections 3.2.3 to 3.2.7) returns a value of cloud base p_B, and CBL top pressure, p_T, between model levels. The adjacent model levels at cloud-top and inversion top were chosen to bracket the computed CBL top pressure, so that the radiating cloud-top is within the CBL. Above the CBL top (p < 790mb), the temperature profile in Figure 6 for this coupled solution follows a moist adiabat through the cloud base temperature, and hence the low level θ_e

3.2.3 *CBL Budgets*

The steady state, horizontally homogenous heat and moisture budgets for the CBL in a subsiding mean flow can be written

$$\omega(T/\theta)(\partial\theta/\partial p) - (g/C_p)(\partial N/\partial p) - g(T/\theta)(\partial F_\theta/\partial p) = 0 \qquad (9a)$$

$$\omega(\partial q/\partial p) - g\partial F_q/\partial p = 0 \qquad (9b)$$

where N is the net outgoing radiation flux, $C_pF_\theta . LF_q$. are the convective fluxes of saturation (liquid water) potential temperature and total water. As a simplification, we shall assume constant divergence, D, through the CBL so that ω is linear, and ignore the variation of (T/θ). Integrating (9) through the CBL from surface, p_O, to inversion top, p_T, then gives

$$\omega_T(\theta_T - \bar{\theta}) - (g\bar{\theta}/C_{p}T)\Delta N_T + gF_{O\theta} = 0 \qquad (10a)$$

$$\omega_T(q_T - \bar{q}) + gF_{Oq} \qquad (10b)$$

where the overbar denotes a CBL average; ω_T, θ_T and q_T are the subsidence, potential temperature and mixing ratio respectively at CBL top; ΔN_T, is the net radiative flux difference across the CBL (typically positive), and $F_{O\theta}, F_{Oq}$ are now the surface fluxes.

Since θ and q lie on a mixing line between (θ_{MO}, q_{MO}) and (θ_T, q_T) for both clear and cloudy profiles, the averages $\bar{\theta}, \bar{q}$ also lie on this mixing line and can be reexpressed as a linear combination with a coefficient α

$$\bar{\theta} = \theta_{MO} + \alpha(\theta_T - \theta_{MO}) \qquad (11a)$$

$$\bar{q} = q_{MO} + \alpha(qT - q_{MO}) \qquad (11b)$$

Given the mixing line, and the specified β's, as well as cloud base and cloud-top, the coefficient α could be computed in (11a), and (11b), and it is typically ≈ 0.25 for a 30% cloud fraction. However, we do not need to compute α. Substituting (11) in (10) gives

$$\omega_{T'}(\theta_T - \theta_{MO}) - (g\bar{\theta}/C_pT)\Delta N_T + gF_{O\theta} = 0 \qquad (12a)$$

$$\omega_{T'}(q_T - q_{MO}) + gF_{Oq} = 0 \qquad (12b)$$

where $\omega_{T'} = (1-\alpha)\omega_T$ is a modified subsidence. This transformation removes the vertical structure represented by $\theta(p), q(p)$ and gives a vertical divergence term involving a reduced subsidence and only *boundary* values for the CBL. We shall use only $\omega_{T'}$, as a parameter representing subsidence. In essence, our bulk CBL model ignores any changes in the internal structure of the CBL by assuming constant values for β and a constant divergence profile. The mixed layer model is a special case with $\beta = \alpha = 0$ and $\theta_{MO} = \bar{\theta}$ Furthermore, if we had not assumed constant divergence in the CBL, than $\bar{\theta}, \bar{q}$ become simply divergence-weighted values, and the value of α is typically reduced

3.2.4. *Surface flux parameterization*

We shall use the bulk aerodynamic formulas to give the surface fluxes

$$F_{O\theta} = \omega_O(\theta_O - \theta_{MO})/g \qquad (13a)$$

$$F_{Oq} = \omega_O(q_o - q_{MO})/g \qquad (13b)$$

where a surface transfer scale has been defined as

$$\omega_O = \rho_O g C_T V_O \qquad (14)$$

where ρ_O, V_O are surface air density and windspeed, and C_T is a surface transfer coefficient. We shall assume saturation at the sea surface temperature (SST) and pressure, so that these give θ_O, and q_O. $(\theta_{MO}\ q_{MO})$ are defined 2mb above the surface. ω_O, proportional to the surface windspeed will be an important *external* parameter in our analyses. $\omega_O = 0.1$ Pa s^{-1} corresponds to $V_O = 6.7\,ms^{-1}$ with $C_T = 1.3x10^{-3}$

3.2.5. *Tropospheric thermodynamic structure.*

Above the CBL, the temperature and moisture profiles are parameterized in a simple way. We assume (following [12]) that the deep convection in the ascending branch of Figure 5 adjusts the tropospheric temperature structure to a moist adiabat. For the coupled solutions the temperature profile follows the moist θ_{es} adiabat through the low level θ_e from CBL top to the tropopause (itself found by the pressure where this θ_{es} adiabat reaches 195K, the specified temperature of the lower stratosphere). For the uncoupled CBL solutions, we break the link to the low level θ_e by specifying this moist adiabat. Although a more refined deep convective adjustment scheme could be used to give a thermal structure closer to that observed (eg., [24]), the moist adiabat is probably satisfactory for *radiative* purposes, because the tropical moisture structure above the CBL is poorly understood [1], and we are not modelling upper level clouds.

The moisture profile above the CBL plays an important role. The bulk radiative cooling of the CBL increases sharply as the mixing ratio above the CBL decreases, and moisture at high levels reduces the bulk cooling of the troposphere. This vertical moisture profile was found by interpolating between values at the CBL top and the tropopause. From the mixing ratio q_T, just above the CBL, we computed a corresponding saturation pressure departure $\mathcal{P}_T = (p^* - p)_T$ The moisture at the tropopause was found by specifying $\mathcal{P}_{TR} = (p^* - p)_{TR}$ For most of the studies we set $\mathcal{P}_{TR} = -30$ mb, which corresponds to roughly 10% relative humidity at (typically) 130mb. The moisture profile between CBL top and the tropopause was then computed by imposing a linear profile of $\mathcal{P}$ with pressure, to give a model profile of q which changes smoothly with q_T. For the uncoupled solutions we explore the sensitivity of the CBL equilibrium to the specification of q_T. We then empirically coupled q_T and the tropospheric moisture to the low level θ_e (Table 1).

TABLE 1. Model coupling between moisture at CBL top and tropospheric θ_{es}

q_T (gKg^{-1})	θ_{es} (K)
4.16	330
4.56	340
4.97	350
5.41	360

[1] noted that the air above the CBL seemed to have subsided on average from a little above the freezing level in the tropical atmosphere. We roughly fitted this by specifying q_T as saturation q_s at -7°C on the tropospheric moist adiabat, θ_{es} (itself equal to the low level θ_e). This couples q_T to θ_{es} so that q_T increases slowly as the troposphere warms. Although this increase is small, it has a significant radiative impact on CBL top.

3.2.6. *Conceptual solution*

The four equations (12a), (12b), (13a) and (13b) appear to have eleven unknowns: $F_{O\theta}$, F_{Oq}, θ_{MO}, q_{MO}, θ_O, q_O, ω_T, ω_O and ΔN_T. Of these ΔN_T will be computed from the radiation model, and ω_O will always be a specified external parameter, related to the surface wind through (14). q_T is specified or modelled as discussed in section (3.2.5). θ_O and q_O are found from the fixed sea surface pressure (1012mb) and SST; which is here specified. For the uncoupled solutions (section 3.3), we shall specify ω_T; while for the coupled solutions (section 3.4), this is determined by a tropospheric energy balance constraint (see 3.2.7). This leaves five unknowns, θ_{MO} and q_{MO}, which give low level θ_e, the surface fluxes $F_{O\theta}$ and F_{Oq}, and θ_T the free tropospheric potential temperature at the CBL top. One more equation is needed for solution, and we shall introduce a constraint on the surface heat flux (see 3.2.7), related to the radiative cooling of the subcloud layer.

The CBL top pressure, p_T, does not appear explicitly in the CBL budget equations (12). However, it can be found from θ_T at the CBL top and the tropospheric θ_{es} above the CBL. For the uncoupled solutions, this θ_{es} adiabat is specified (Section 3.2.5), while for the coupled solutions, it is linked to the low level θ_e, and we solve

$$\theta_{es}(\theta_T, p_T) - \theta_e(\theta_{MO}, q_{MO}) \tag{15}$$

for p_T. Thus we find from θ_T, the equilibrium boundary layer depth, for which the radiative cooling is balanced by the surface heat flux, and the subsidence into the CBL of warm air of known θ_{es} from the troposphere above.

3.2.7 *Energy balance closures*

These are crucial constraints which give radiative convective-equilibrium.

Subcloud layer energy balance. One simple constraint, used by [12], and [2] is to specify the surface Bowen ratio

$$b = C_p F_{O\theta} / L F_{Oq} \tag{16}$$

and investigate the sensitivity to b. Measurements over the oceans have shown b ≈ 0.07 for the undisturbed CBL ([16], [25], [26],[18]. However the dependence of cloud-base and cloud-top on b is large (see [3]), so that the specification of b is a limitation.

In disturbed weather, cooling by subcloud evaporation of rain is known to increase the surface Bowen ratio ([27], [28],[29]), but little is known about its variability in the undisturbed boundary layer Clearly, however, in equilibrium over a uniform ocean, it is the radiative cooling of the subcloud layer that maintains an air-sea temperature difference, and hence a positive surface heat flux. So we decided to use a simple closure for the surface heat flux, and then to calculate the Bowen ratio b using (16). The equilibrium subcloud layer energy balance (neglecting the subsidence term, which is well over an order of magnitude smaller than $F_{O\theta}$) is

$$F_{O\theta} - F_{B\theta} + \Delta N_B = 0 \tag{17a}$$

Betts [21] proposed the closure for the subcloud layer

$$F_{B\theta} = -kF_{O\theta} \quad \text{with } k \approx 0.25 \tag{18}$$

substituting (18) in (17a) gives

$$C_p F_{O\theta} = -\Delta N_B/(1+k) \tag{17b}$$

This couples the surface heat flux directly to the radiative cooling for the subcloud layer, which we can compute. Observational studies have shown a negative sensible heat flux at cloud base (*LeMone and Pennell* [30]). However (18) is not well established for the subcloud layer, and it is usually used as a closure on virtual heat fluxes (see [3]), so we can only guess that $0.5 < (1+k)^{-1} < 1.0$ We decided to use k = 0.25 or $(1+k)^{-1} = 0.8$ Our results are not very sensitive to k. With this closure (17b), the surface heat flux and Bowen ratio (from (16)) decrease with increasing cloud fraction, as the radiative cooling of the subcloud layer decreases.

Tropospheric energy balance. The atmospheric energy balance averaged over the tropics can be written

$$C_p F_{O\theta} + LF_{Oq} = \Delta N_{TR} + \delta N_{uc} + X_A \tag{19}$$

where ΔN_{TR} is the net radiative flux difference between surface and tropopause, X_A is the atmospheric export of energy out of the tropics, and δN_{uc} is the perturbation to the radiative flux divergence associated with upper level clouds. We shall neglect upper clouds and the atmospheric export by setting

$$\delta N_{uc} + X_A \approx 0 \tag{20}$$

to give

$$C_p F_{Oq} + LF_{Oq} = \Delta N_{TR} \tag{21}$$

This is the closed tropical model of [12] and [2]. Upper clouds heat the tropics, and the atmospheric export to mid-latitudes cools, so that although the two terms in (13) are each significant, (≈ 20-30 W m^{-2}, averaged over the tropics: *Ramanathan*, 1987 [31]), they are of opposite sign, with the result that (20) is a fair approximation. Clearly however, (20) is a serious limitation for climate studies.

Eq (21) will be used for the troposphere coupled solutions to give the subsidence parameter $\omega_{T'}$. The method of solution follows [2]. We rewrite (12b), and (13b) as

$$gF_{Oq} = \omega_O(q_O - q_{MO}) = \omega_N(q_O - q_T) \tag{22}$$

where

$$\omega_N = \omega_O\omega_{T'}/(\omega_O + \omega_{T'}). \tag{23}$$

This directly links the surface moisture flux to the q difference between surface and free atmosphere (*Betts* [32]). Then substituting (16) and (21) in (22), we find

$$\omega_N = g\Delta N_{TR}/(1+b)L(q_O - q_T) \tag{24}$$

This gives the bulk transfer scale, ω_N, (and $\omega_{T'}$ from (23)) from the bulk tropospheric cooling ΔN_{TR}. This computation of ω_N is the crucial step in finding our tropospherically coupled solutions. We then solve (22) for F_{Oq} and q_{MO}. The θ budget can also be expressed in terms of ω_N by rearranging (12a), using (23), to give

$$gF_{O\theta} = \omega_O(\theta_O - \theta_{MO}) = \omega_N(\theta_O - \theta_T) + (1 - \omega_N/\omega_O)(g\theta/CpT)\Delta N_T \tag{25}$$

Given ω_N from (24), and $F_{O\theta}$ from (17b), (25) can be solved for θ_{MO} and θ_T. Cloud-base and the low level θ_e are found from θ_{MO}, q_{MO}: these give the tropospheric moist adiabat using (15), and hence p_T from θ_T.

3.3 CBL EQUILIBRIUM : UNCOUPLED SOLUTIONS

In this section we shall present results for the CBL equilibrium for a given SST and given troposphere above the CBL. These represent the equilibrium response of the CBL to diurnally averaged radiative forcing on timescales of order a day. We call these *uncoupled* solutions because the upper tropospheric temperature and moisture, and subsidence at CBL top will be specified rather than coupled to the low level θ_e and the tropospheric radiative budget (Eq 21). In the following section 3.4, we shall show solutions in which the CBL is coupled to the troposphere and constraint (21) is used.

For the uncoupled CBL solutions, there are many external variables, and we shall only show the sensitivity to two. We shall vary sea surface temperature, and surface wind speed about the coupled solution parameter set, given in Table 2. Since the radiative fluxes depend on the thermodynamic structure, the method of solution was to iterate the system of equations to convergence. We shall present three key parameters to represent the equilibrium CBL: cloud-base pressure, p_B, and low level θ_e derived from θ_{MO} and q_{MO}; and cloud-top pressure, p_T.

3.3.1 *CBL structure as a function of SST*

Figure 7 shows the dependence of CBL structure, represented by cloud-base, cloud-top

(solid lines) and lowest level θ_e (heavy dashes) on SST, with fixed surface wind speed.

TABLE 2. Model parameters: Base set.

Solar zenith angle	51.74°
Surface albedo	0.07
Incoming SW flux	1360.3 W m^{-2}
CBL parameters	
cloud	β_c = 0 (subcloud); 0.6 (cloud layer)
environment	β_u = 0.2 (subcloud); 1.2 (cloud layer)
Subcloud layer closure parameter	k = 0.25
Tropopause subsaturation	$\mathcal{P}_{TR}$ = −30 mb
Mixing ratio just above CBL	q_T = 4.8 g kg^{-1}
Ocean surface temperature	SST = 300 K
Surface wind parameter	ω_O = 0.1 Pa s^{-1} (≈6.7 m s^{-1})
Tropospheric	θ_{es} = 347 K
Subsidence parameter	$\omega_{T'}$ = 0.05 Pa s^{-1}
Cloud fraction	= 25%

For an SST of 300K typical of the tropical oceans, we obtain an equilibrium cloud-base near 950mb, cloud-top (and inversion top) near 800mb and a low level θ_e of 347K. This is in good agreement with the observed mean CBL structure in the tropics. With increasing SST, cloud-base barely changes, while the equilibrium cloud-top inversion rises rapidly, so that the uncoupled model predicts a deeper CBL over warmer oceans. The steep increase in θ_e with SST is of great importance. It illustrates the tight coupling of the boundary layer to the ocean. Ocean surface θ_{es} (light dashes) also increases with SST, but the subcloud θ_e remains about 14-24K lower (over this temperature range), corresponding to saturation near 950mb at the top of the dry adiabatic subcloud layer.

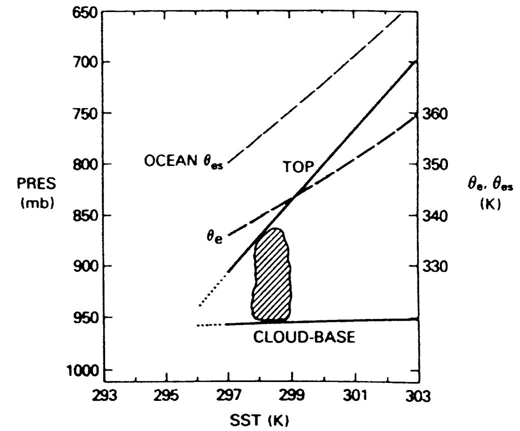

Figure 7. Uncoupled CBL solutions for cloud-base and CBL top (solid lines) and low level θ_e (long heavy dashes: scale on right) as a function of SST, for surface wind parameter ω_O= 0.1. θ_{es} for the sea surface is shown as long light dashes.

Figure 7 shows that for a fixed subsidence parameter and fixed upper troposphere, cloud-top is quite sensitive to SST. The cloud layer disappears around an SST of 296K (see dotted extropolation: our model cannot resolve cloud layers ≤ 20mb in depth). This is a greater sensitivity than shown by *Albrecht* [33] [34], who specified constant divergence (so that as CBL top increases, ω_T does also). These equilibrium solutions satisfy only the CBL energy balance constraints. The tropical upper troposphere has a fixed temperature structure on the θ_{es} = 347K moist adiabat, corresponding to the low level θ_e from the fully coupled solution with an SST = 300K.

Figure 7 suggests that if the SST is locally above 300K, then the CBL equilibrium will give θ_e > 347K, sufficient to give deep convective instability. The relationship between tropical SST and deep convection was noted by *Gadgil et al.* [35]. Studies of tropical convection (*Graham and Barnett* [36]) have shown that there is a sharp change in convection regimes above a critical SST, which is about 27.5°C for much of the Indian and Pacific oceans, and somewhat lower (<27°C) for the Atlantic. They found that deep convection requires an SST above this threshold, while below it, only shallow CBL clouds are typically observed. Figure 7 suggests a simple explanation of this. θ_{es} for the deep troposphere and the low level capping inversion is typically in the range 347-350K in the tropics. Our equilibrium CBL θ_e reaches 347K for an SST of 27°C and 350K for an SST of 27.7°C. This also suggests that the reason for the well-known threshold for hurricane formation only at SST's > 26.5°C (299.7K) (*Palmen* [37]) is directly related as well to the boundary layer equilibrium θ_e, which for larger SST's exceeds the mean θ_{es} of the deep tropical atmosphere.

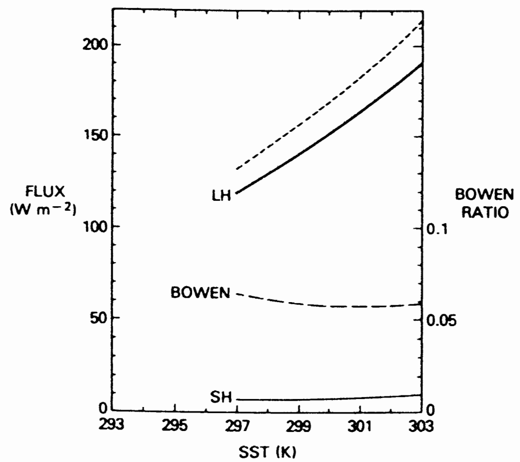

Figure 8. Surface sensible and latent heat fluxes (solid lines) and Bowen ratio (long dashes) for uncoupled CBL solutions as a function of SST, for ω_O = 0.1. The latent heat flux for a higher wind-speed ω_O = 0.15, approximately 10 m s^{-1}) is shown as short dashes.

Figure 8 shows the increase in the equilibrium surface sensible and latent fluxes (solid lines) with SST. The sensible heat flux increases +0.6 Wm^{-2}K^{-1}, and the latent heat flux by +11.7 Wm^{-2} K^{-1}, as SST increases. There is little change in the surface Bowen ratio (long dashes) of ≈ 0.06. This rate of increase of the total surface heat flux with SST is double that of the tropospherically coupled CBL discussed in section 3.4 For comparison, a simple ocean - atmosphere interaction model (which *assumes* constant relative humidity (of 73.8%) and wind speed) has a slope of latent heat flux of 9.2 Wm^{-2} K^{-1} near 300K. The short dashed line on Figure 8 shows latent heat flux with SST for a higher windspeed ω_O = 0.15 Pa s^{-1}).

3.3.2 *The effect of surface wind-speed*

We then kept SST fixed at 300K and varied surface wind speed. Figure 9 shows that with increasing wind-speed, cloud-base descends, and cloud-top rises to give a deeper CBL. As surface wind falls, the subcloud layer cools and dries in response to the subsidence above, and the cloud layer gets thinner, until at low wind-speeds ≈ 3ms^{-1}, it is no longer possible to maintain an equilibrium cloudy boundary layer. θ_e increases with wind-speed, rapidly at low windspeeds, with a more asymptotic behavior at higher wind speeds towards the θ_{es} of the ocean (365K at an SST of 300K; shown as long light dashes). This equilibrium suggests that regions of climatically higher wind speed should have climatically higher θ_e, and more deep convection. It also confirms that in the equilibrium hurricane (*Emanuel* [38]), the increase in surface wind will tend to drive the CBL to higher θ_e.

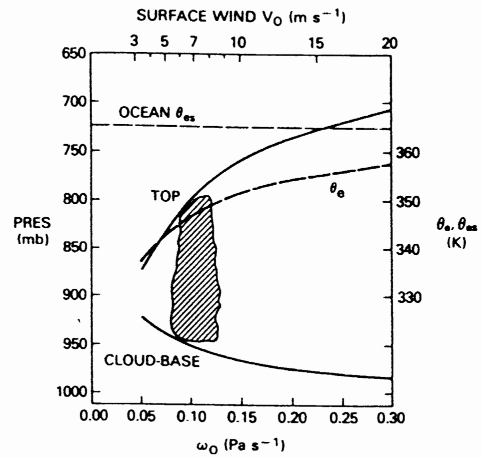

Figure 9. As Fig 7 for fixed SST = 300K as a function of surface wind. Ocean θ_{es} shown as long light dashes.

Figure 10 shows the response of the surface fluxes to surface wind changes as the boundary layer structure adjusts. With increasing wind, the latent heat flux increases and the sensible heat flux decreases (as the air-sea temperature difference becomes very small: Figure 11), and correspondingly the Bowen ratio falls. The sea-air Δq difference also falls rapidly with increasing wind-speed (Figure 11), so that the increase in the LH flux with ω_O is much less steep than if Δq or relative humidity remained constant. The dotted line in Figure 10 indicates for comparison the linear change of latent heat flux with ω_O, for constant Δq, corresponding to the values at ω_O = 0.1. In section 3.4, we shall show that the coupled solutions have even less of an increase with windspeed.

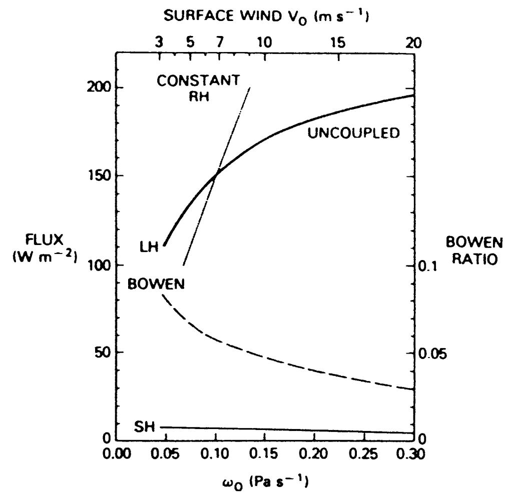

Figure 10. As Fig 8 as a function of surface wind parameter ω_O. Dotted line shows the slope of latent heat flux with surface wind for fixed relative humidity.

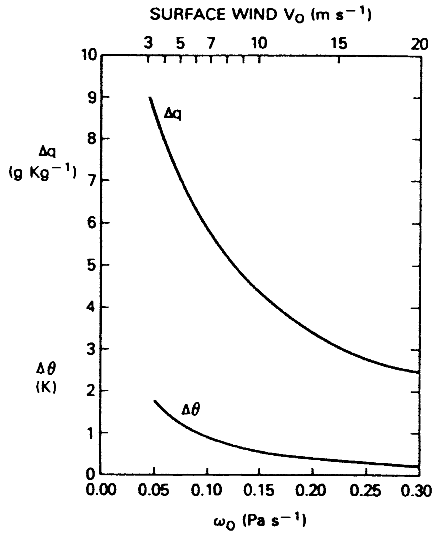

Figure 11. Sea-air difference of mixing ratio (Δq) and potential temperature ($\Delta\theta$) as a function of surface wind for uncoupled equilibrium solutions.

3.4. COUPLED SOLUTIONS SATISFYING TROPOSPHERIC ENERGY BALANCE

We now explore how the CBL equilibrium is altered by introducing constraint (21) for tropospheric energy balance, as well as a tropospheric moist adiabat linked to the low level

θ_e We shall separately couple the moisture, q_T, above the CBL (as in Table)1 to the low level θ_e

TABLE 3. Model solution for SST = 300 K, and 25% cloud fraction.

Input parameters	
p_O	1012 mb
SST	300 K
ω_O	0.1 Pa s^{-1}
Cloud fraction	25%
$\mathcal{P}_{TR}$	−30 mb
Model solution	
p_B	954 mb
p_T	796 mb
θ_e	346.8 K
$\theta_O - \theta_{MO}$	0.84 K
$q_O - q_{MO}$	5.9 g kg^{-1}
RH	74%
$F_{OCp\theta}$	9 W m^{-2}
F_{OLq}	150 W m^{-2}
Bowen ratio	0.06
$\omega_{T'}$	0.049 Pa s^{-1}
ω_N	0.033 Pa s^{-1}
θ_T	307.0 K
q_T	4.8 g kg^{-1}
θ_{eT}	322 K
ΔN_B	11 W m^{-2}
ΔN_T	52 W m^{-2}
ΔN_{TR}	158 W m^{-2}

3.4.1. *Basic solution with coupled troposphere*
Our steady state model solution for a tropical mean SST of 300K with a coupled troposphere is given in Table 3. The values for cloud-base near 950 mb, cloud-top near 800 mb, low level θ_e near 347K and surface sensible and latent heat fluxes of 9 and 150 Wm^{-2} respectively are quite close to observed climatic values ([16] [1]). This gives us confidence in both the basic model structure and assumptions, and in the radiation code.

3.4.2. *Sensitivity to troposphere moisture*
Figure 12 shows the response of the coupled CBL to changing q_T (the moisture at CBL top). The change of cloud-base and low level θ_e with increasing q_T are considerably reduced, while the fall of cloud-top is amplified. This is becaus ω_N (and $\omega_{T'}$) increases as $(q_O$-$q_T)$ decreases in Eq (24), despite a small fall in the tropospheric radiational cooling ΔN_{TR}. Figure 12 shows that the primary effect of coupling q_T to the low level θ_e (Table 1) will be on cloud-top, with little impact on cloud-base or low level θ_e. In particular, the rise of q_T with θ_e will reduce the rise of cloud-top.

3.4.3. *Sensitivity to SST.*
Figure 13 shows the dependence of CBL structure, represented by cloud-base, cloud-top and lowest level θ_e over a 10K range of SST for the tropospherically coupled system. With increasing SST, cloud-base now falls steadily, while the equilibrium cloud-top inversion rises (solid lines). Three cloud-top curves are shown. The solid line (labeled coupled),

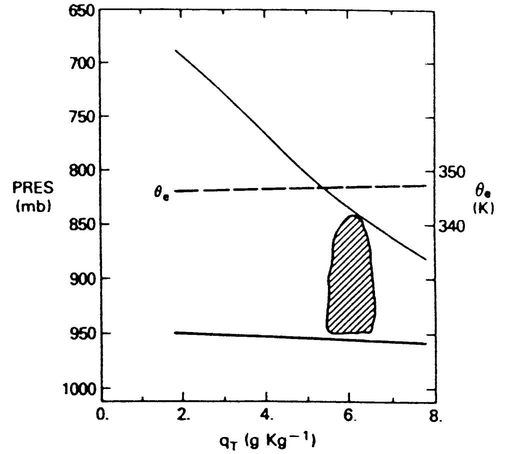

Figure 12. As Fig 7 as a function of mixing ratio above inversion and with coupled tropospheric θ_{es} and CBL top subsidence.

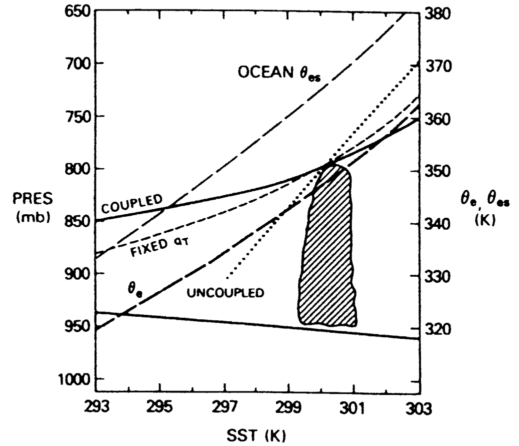

Figure 13. As Fig 7 for coupled tropospheric θ_{es}, q_T and subsidence: cloud-base and CBL top as solid lines, θ_e as heavy dashed lines. Short dashes show cloud-top for fixed q_T, but coupled θ_{es} and subsidence. Dotted line is CBL top for uncoupled solution from Fig 7.

which shows the slowest CBL deepening with increasing SST is for the fully coupled troposphere with the moist adiabat θ_{es}, and moisture q_T both coupled to the low level θ_e, and the subsidence coupled to the tropospheric cooling through (24) and (23). The dashed line has q_T fixed at 4.8 g Kg^{-1}, but coupled subsidence and temperature (moist adiabat θ_{es} = low level θ_e), and the dotted line is the steep rise of cloud top with SST for the uncoupled solutions (from Figure 7). We see that, with greater coupling, the CBL depth changes more slowly with SST. With a coupled troposphere, the cloud top subsidence actually *decreases*

with increasing SST, because $(q_O - q_T)$ increases faster than ΔN_{TR} in (24). However, cloud top θ_T increases so rapidly with θ_{es}, (at constant p_T), that the cloud top rise is reduced. The coupling of q_T to the low level θ_e further reduces the rise of cloud top.

The rise of θ_e (heavy dashes) with SST is a little steeper than the uncoupled solution in Figure 7. The coupling of the boundary layer to the ocean is a little tighter with the CBL θ_e ranging from 14-21K below the θ_{es} of the ocean (long light dashes) over the SST range from 293-303K.

The corresponding wet-bulb depression at the surface varies very weakly with SST A simple formulae for the atmospheric low level T_{wO} (at this windspeed 6.7 ms^{-1}) is

$$T_{wO} = T_O - 3.6\,(1 + 0.008\,(300 - T_0)) \tag{26}$$

The low level equilibrium θ_e (saturation at (p_O, T_{wO}) can be found from (26) to an accuracy of $\approx$ 0.2K for $293 < T_O < 303$K.

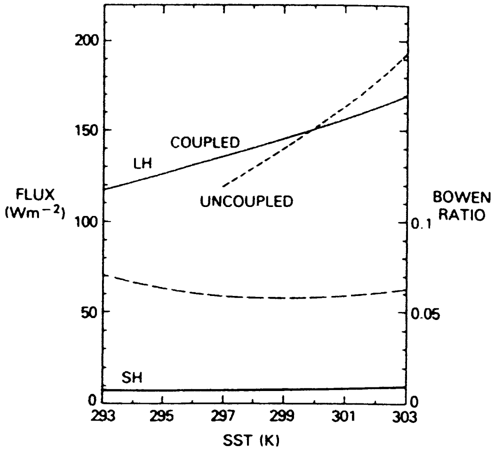

Figure 14. As Fig 8 for tropospherically coupled solution. Short dashed line is latent heat flux from Fig 8.

Figure 14 shows the increase in the equilibrium surface sensible and latent fluxes with SST for the fully coupled solution (solid lines). For 297 < SST < 303K the sensible heat flux increases +0.5 Wm^{-2}K^{-1}, and the latent heat flux by +6.6 $Wm^{-2}\,K^{-1}$ The surface Bowen ratio changes weakly with SST. This rate of increase of the latent heat flux with SST is about half that of the uncoupled CBL, shown dashed (from Figure 8). The rate of increase in the total surface heat flux is now almost identical to the rate of increase in the surface emittance given by differentiating Planck's law.

$$\begin{aligned}\delta E/\delta T &= 4\sigma T^3\\ &= 6.1\ \mathrm{Wm^{-2}K^{-1}}\ \text{at } 300\mathrm{K}\end{aligned}$$

This may reflect the tight coupling to the SST of the CBL structure and the radiative emission to space.

3.4.4. *Sensitivity to surface wind-speed*

Figure 15 shows that with increasing wind-speed, cloud-base descends, and cloud-top rises to give a deeper CBL. Three cloud-top curves are again shown. The solid line for tropospherically coupled subsidence, θ_{es} and q_T again shows the least variation with surface wind speed; the short dashed line with q_T fixed (but coupled subsidence and θ_{es}) shows more deepening of the CBL with wind speed, and the dotted curve for the uncoupled solutions (from Figure 9) shows the sharpest slope of cloud-top pressure with windspeed. Once again the increase in cloud-top θ_T, associated with rising θ_{es}, dominates over a weak decrease in cloud-top subsidence in Eq (12a), so that the rise of cloud-top with surface wind is reduced for a coupled tropospheric temperature and subsidence. The coupling of q_T to θ_e further reduces the deepening of the CBL.

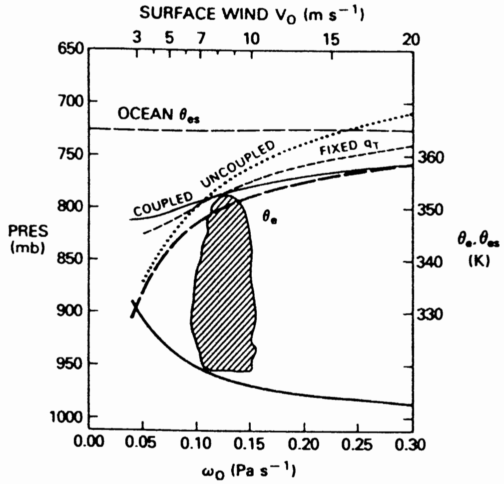

Figure 15. As Fig 9 for tropospheric coupled solution. Solid lines are for coupled θ_{es}, q_T and subsidence; short dashed line is for fixed q_T, but coupled θ_{es} and subsidence; and dotted line is CBL top for uncoupled solution from Fig 9.

There is a singularity at low wind-speeds $\approx 3ms^{-1}$, where it is no longer possible to maintain an equilibrium cloudy boundary layer. As surface wind falls, the subcloud cools and dries in response to the subsidence above, and the cloud layer gets thinner. The change of θ_e with wind speed is similar to the uncoupled solution in Figure 9. θ_e increases with wind-speed rapidly at low windspeeds, with a more asymptotic behavior at higher wind speeds towards the θ_{es} of the ocean (light long dashes). This equilibrium again suggests that regions of climatically higher wind speed should have climatically higher low level θ_e. This could be tested using climatic data sets.

Figure 16 shows the response of the surface fluxes to surface wind changes (solid lines) with coupled θ_{es}, q_T and subsidence. With increasing surface wind, latent heat increases and the sensible heat flux decreases (as the air-sea temperature difference falls), and correspondingly the Bowen ratio (long dashes) falls as in Figure 10. The sea-air Δq difference (not shown) falls more rapidly with increasing wind-speed than in Figure 11 for the uncoupled CBL, so that the increase in the LH flux with ω_O is less than for the uncoupled solution; shown dashed (from Figure 10). The dotted line again indicates the change with ω_O for constant Δq corresponding to the values at $\omega_O = 0.1$ We see that with increasing coupling the rise of LH with windspeed becomes much less steep.

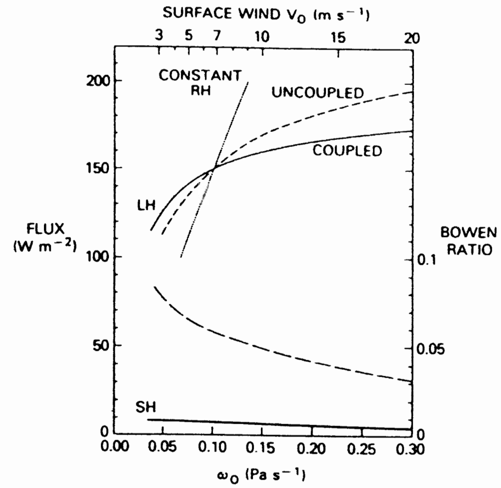

Figure 16. As Fig 10 for tropospheric coupled solution; compared with uncoupled solution (short dashes), and constant relative humidity solution (dotted).

3.4.5. *Tropopause height*

The coupled solutions give almost trivially the pressure of the tropopause where the θ_{es} moist adiabat reaches 195K, the fixed temperature of the lower stratosphere (as in [12]). The tropopause pressure falls from 177 to 115 mb as SST increases from 293K to 303K (θ_e increasing from 320 to 361K). The change with increasing windspeed is similar

3.4.6. *Discussion of tropospheric coupled solutions.*

We have seen that the introduction of tropospheric coupling has two significant impacts on the CBL structure and fluxes. One is to reduce the deepening of the CBL with increasing SST and surface wind. This effect is dominated by two processes: the increase of cloud-top θ_{es} and q_T with low level θ_e. The second is the reduction of the increase of the surface latent heat flux with SST and wind speed. This is caused by changes in the bulk transfer parameter ω_V given by (24). The surface Bowen ratio changes only weakly with SST, but falls rapidly with increasing wind speed, as the CBL adjusts to a lower cloud-base as the subcloud layer moistens.

3.4.7. *Relationship of CBL depth to SST*

Figure 13 shows how the increase in CBL depth with increasing SST is reduced by greater tropospheric coupling. An earlier model by Albrecht [39]which specified divergence and CBL radiative cooling, gave a slope of CBL depth with SST intermediate between our uncoupled and partially coupled solutions (dotted and short dashed lines in Figure 13). In an observational study along downstream trajectories in the eastern North Pacific towards Hawaii [15], the observed mean slope and height of the inversion base agrees well with the coupled solution for CBL top (solid line in Figure 13) His inversion top is however 30-40 mb higher Although our model was constructed for a "global tropics", and does not include the lag associated with horizontal advection over a warmer SST, it represents solutions for any large region of the tropics for which the energy balance closure (21) is approximately satisfied. It seems likely that the rise of mean inversion height along the NE Pacific tradewind trajectory described by [24], [14] and [15] is primarily due to the rise in SST

4. Conclusions

We first discussed Trade-wind cumulus equilibrium. We showed how the surface fluxes, the radiatively driven subsidence, internal radiative cooling and the thermodynamic structure of the CBL are closely coupled. This CBL equilibrium controls the mean thermodynamic structure of the Tropics.

We then discussed this surface flux and CBL equilibrium on 2 timescales using a coupled radiative-convective boundary layer model and energy balance constraints. In Section 3.3 (Figures 7-11), we showed the "uncoupled" CBL solutions: those with a specified SST, tropospheric thermodynamic structure and cloud-top subsidence parameter These satisfy radiative equilibrium only for the CBL. They show an increase of CBL depth with increasing SST and a tight coupling of the low level θ_e to the SST. The threshold for deep convection associated with SST's > 27.5°C, observed in much of the Pacific and Indian Oceans [26]), is probably related to low level θ_e exceeding the deep tropospheric θ_{es} above this SST. With increasing surface wind, cloud-base falls, while θ_e and cloud-top both increase. The latent heat flux increases nearly linearly at 11.1 $Wm^{-2} K^{-1}$ with SST, while the response to increasing wind is quite non-linear, as the CBL structure adjusts. The slope near 6.7 ms^{-1} is only one third of the linear slope assuming constant relative humidity (Figure 10). Increasing the subsidence parameter suppresses the CBL, reduces θ_e and increases the surface latent heat flux for constant surface wind and SST. Cloud-top is sensitive to the moisture above, which controls the radiative cooling of the CBL. The coupling of the sensible heat flux to the radiative cooling of the subcloud layer gives a tightly constrained sensible heat ≈ 8-10 Wm^{-2}, and a Bowen ratio ≈ 0.06 for constant surface wind speed, similar to observed values for the undisturbed Trades. However, with increasing wind speed, cloud base falls, and with it the Bowen ratio falls also.

In Section 3.4, we coupled the subsidence (ω_T) at CBL-top to the deep tropospheric net radiative cooling (through a parameter ω_N); and the tropospheric temperature (θ_{es}) and moisture structure (q_T) to the low level θ_e. The model solutions of cloud-base near 950 mb, cloud-top and CBL top near 800 mb and a low level θ_e of 347K are close to the tropical mean for an SST of 300K. This gives us confidence in both the basic model structure and the radiation code. There are two major impacts of "tropospheric coupling" on the CBL structure and fluxes. The deepening of CBL with SST and surface wind was reduced significantly; first by the coupling of ω_T, and θ_{es}, and still further by the coupling of q_T. The surface latent heat flux increase with SST was halved to 5.6 W $m^{-2} K^{-1}$; giving a total surface heat flux increase close to the slope of the Planck function with SST. The slope of the latent heat flux with surface wind was almost halved to 4 W m^{-3} s by introducing tropospheric coupling. In this case the surface fluxes can only increase as the CBL moistens and the longwave cooling of the troposphere increases. The extension of this equilibrium

model to the energy balance at the ocean surface, which gives the equilibrium SST, is discussed in [3], and the coupling to an ocean mixed layer in [23].

5. Acknowledgements

This research has been supported by NSF under a series of Grants spanning many years, and by contracts from NASA-GSFC Much of this work has been adapted from the author's cited publications for which the original publisher holds the copyright.

6. References

1 Betts, A. K., and Albrecht, B.A. (1987) Conserved variable analysis of boundary layer thermodynamic structure over the tropical oceans. *J. Atmos Sci.* **44**, 83-99.
2. Betts, A. K. and Ridgway, W. (1988) Coupling of the radiative, convective and surface fluxes over the equatorial Pacific. *J. Atmos. Sci.* **45**, 522-536.
3. Betts, A. K. and Ridgway, W. (1989) Climatic equilibrium of the atmospheric convective boundary layer over a tropical ocean. *J. Atmos. Sci.* **46**, 2621-2641.
4. Betts, A. K. (1975) Parametric Interpretation of Trade Wind Cumulus Budget Studies. *J. Atmos. Sci.* **32**, 1934-1955.
5. Betts, A. K. (1982a) Saturation point analysis of moist convective overturning. *J. Atmos. Sci.* **39**, 1484-1505.
6. Betts, A. K. (1982b) Cloud thermodynamic models in saturation point coordinates. *J. Atmos. Sci.* **39**, 2182-2191.
7. Betts, A. K. (1984) Boundary layer thermodynamics of a High Plains severe storm. *Mon. Wea. Rev.* **112**, 2199-2211.
8. Betts, A. K. (1985a) Mixing line analysis of clouds and cloudy boundary layers. *J. Atmos. Sci.* **42**, 2751-2763.
9. Betts, A. K. (1985b) Vector representation of Trade cumulus thermodynamic fluxes. *Mon. Wea. Rev.* **13**, 2173-2175.
10. Betts, A.K. (1992) FIFE Atmospheric Boundary Layer Budget Methods. *J.G.R.* **97**, 18523-18531.
11. Firestone, J.K., and Albrecht, B.A. (1986) The structure of the atmospheric boundary layer in the central equatorial Pacific during January and February of FGGE. *Mon. Wea. Rev.* **114**, 2219-2231.
12. Sarachik, E. S. (1978) Tropical sea surface temperature: an interactive one-dimensional atmosphere ocean model. *Dyn. Atmos. Oceans* **2**, 455-469.
13. Riehl, H., Yeh, T.C., Malkus, J.S. and LaSeur, N.E. (1951) The North-east trade of the Pacific Ocean. *Quart. J. Roy. Meteor. Soc.* 77, 598-626.
14. Malkus, J.S. (1956) On the maintenance of the tradewinds. *Tellus* **8**, 335-350.
15. Neiburger M. (1960) The relationship of air mass structure to the field of motion over the Easter North Pacific in Summer. *Tellus* **12**, 31-40.
16. Holland, J. Z., and Rasmusson, E. (1973) Measurements of the atmospheric mass energy and momentum budgets over a 500 kilometer square of tropical ocean. *Mon. Wea. Rev.* **101**, 44-55.
17. Nitta, T., and Esbensen, S. (1974) Heat and moisture budgets using BOMEX data. *Mon. Wea. Rev.* **102**, 17-28.
18. Augstein, E., Riehl, H. Ostapoff, F. and Wagner, V. (1973) Mass and energy transports in an undisturbed Atlantic Trade wind flow. *Mon. Wea. Rev.* **101**, 101-111.
19. Betts, A. K. (1989) Idealized stratocumulus models and cloud layer thickness. *Tellus* **41A**, 246-254.
20. Miller, M.J., Beljaars, A.C.M. and Palmer, T.N. (1993) The sensitivity of the ECMWF model

to the parameterization of evaporation from the tropical oceans. *J. Clim.* **5**, 418-434

21 Betts, A. K., (1973) Non-Precipitating Convection and Its parameterization. *Quart. J. Roy Meteor. Soc.* **99**, 178-196.

22 Schubert, W H., J S. Wakefield, E. J. Steiner, and S. K. Cox (1979) Marine stratocumulus convection. Part I· Governing equations and horizontally homogeneous solutions. *J Atmos. Sci* **36**, 1286-1307

23. Sui,C.-H., Lau, K.-M. and Betts, A.K. (1991) An equilibrium model for the coupled ocean-atmosphere layer in the tropics. *J. Geophys. Res.* **96**, 3151-3163.

24 Betts, A. K. (1986) A new convective adjustment scheme. Part I: Observational and theoretical basis. *Quart. J. Roy. Meteor. Soc.* **112**, 677-692.

25. Pond,S., G.T. Phelps, J.E. Paquin, G. McBean, and R.W. Stewart (1971) Measurements of the turbulent fluxes of momentum moisture and sensible heat over the ocean. J. Atmos. Sci., 28, 901-917.

26. Paulson, C.A., E. Levitt, and R.G. Fleagle (1972) Air-sea transfer of momentum, heat and water determined from profile measurements during BOMEX. *J. Phys. Ocean.* **2**, 487-497.

27. Malkus, J.S. (1962) Large-scale interactions. Chapter 4 in The Sea. Vol. 1: Ideas and Observations on Progress in Study of the Sea. M.N. Hill, Ed., *Wiley-Interscience*, 88-294.

28. Augstein, E. (1978) The atmospheric boundary layer over the tropical oceans in "Meteorology over the Tropical Oceans." Ed. D.B. Shaw. *Royal Meteor. Soc.*, 1978 73-104.

29. Betts, A. K., and Simpson, J. (1987) Thermodynamic budget diagrams for the hurricane subcloud layer. *J. Atmos. Sci.* **44**, 842-849.

30. Lemone M.A., and Pennell, W.T. (1976) The relationship of tradewind cumulus distributuin tosubcloud layer fluxes and structure. *Mon. Wea. Rev.* **104**, 524-539.

31. Ramanathan, V. (1987) The role of earth radiation budget studies in climate and general circulation research. *J. Geophys, Res.* **92**, 4075-4095.

32. Betts, A.K. (1983) Thermodynamics of mixed stratocumulus layers; saturation point budgets. *J. Atmos. Sci.* **40**, 2655-2670.

33. Albrecht, B.A. (1979) A model of the thermodynamic structure of the trade wind boundary layer: Part II Applications. *J. Atmos. Sci.* **36**, 90-98.

34. Albrecht, B. A., A. K. Betts, W. Schubert and S. K. Cox (1979) A model of the thermodynamic structure of the trade-wind boundary layer: Part I Theoretical formulation and sensitivity tests. *J. Atmos. Sci.*, **35**, 73-89.

35. Gadgil, S., Joseph, P.V. and Joshi, N.V. (1984) Ocean-atmosphere coupling over monsoon regions. *Nature* **312**, 141-143.

36. Graham, N.E., and Barnett, T.P. (1987) Sea surface temperature, surface wind divergence and convection over the tropical oceans. *Science* **238**, 657-659.

37. Palmen, E. (1948) On the formation and structure of tropical cyclones. *Geophysica* **3**, 26-28.

38. Emanuel, K. A. (1988) The maximum intensity of hurricanes. *J. Atmos. Sci.*, **45**, 1143-1155.

39. Albrecht, B.A. (1984) A model of downstream variations of the thermodynamic structure of the trade winds. *Tellus*, **36A**, 187-202.